To be Submitted to the ApJ

The *CHANDRA* HETGS X-ray Grating Spectrum of η Carinae

M. F. Corcoran[1,2], J. H. Swank[2], R. Petre[2], K. Ishibashi[3], K. Davidson[4], L. Townsley[5], R. Smith[6], S. White[7], R. Viotti[8], A. Damineli[9]

ABSTRACT

η Carinae may be the most massive and luminous star in the Galaxy and is suspected to be a massive, colliding wind binary system. The *CHANDRA* X-ray observatory has obtained a calibrated, high-resolution X-ray spectrum of the star uncontaminated by the nearby extended soft X-ray emisssion. Our 89 ksec *CHANDRA* observation with the High Energy Transmission Grating Spectrometer (HETGS) shows that the hot gas near the star is non-isothermal. The temperature distribution may represent the emission on either side of the colliding wind bow shock, effectively "resolving" the shock. If so, the pre-shock wind velocities are ~ 700 and ~ 1800 km s^{-1} in our analysis, and these velocities may be interpreted as the terminal velocities of the winds from η Carinae and from the hidden companion star. The forbidden-to-intercombination (f/i) line ratios for the He-like ions of S, Si and Fe are large, indicating that the line forming region lies far from the stellar photosphere. The iron fluorescent line at 1.93Å, first detected by *ASCA*, is clearly resolved from the thermal iron line in the *CHANDRA* grating spectrum. The Fe fluorescent line is weaker in our *CHANDRA* observation than in any of the *ASCA* spectra. The *CHANDRA* observation also provides an uninterrupted high-time resolution lightcurve of the stellar X-ray emission from η Carinae and suggests that there was no significant, coherent variability during the *CHANDRA* observation. The η Carinae *CHANDRA* grating spectrum is unlike recently published X-ray grating spectra

[1]Universities Space Research Association, 7501 Forbes Blvd, Ste 206, Seabrook, MD 20706

[2]Laboratory for High Energy Astrophysics, Goddard Space Flight Center, Greenbelt MD 20771

[3]National Research Council, Laboratory For Astronomy and Space Physics, Goddard Space Flight Center, Greenbelt, MD 20771

[4]Astronomy Department, University of Minnesota, Minneapolis, MN, 55455

[5]Department of Astronomy, Pennsylvania State University, State College, PA

[6]Harvard-Smithsonian Center for Astrophysics, Cambridge, MA

[7]Department of Astronomy, University of Maryland, College Park, MD, 20742

[8]Istituto di Astrofisica Spaziale, CNR, Area di Ricerca Tor Vergata, 00133 Roma, Italy

[9]Instituto Astronômico e Geofisico da USP,Av. Miguel Stefano 4200, 04301-904 São Paulo, Brazil

of single massive stars in significant ways and is generally consistent with colliding wind emission in a massive binary.

Subject headings: η Carinae, stars: individual (η Carinae), stars: early-type, X-rays:stars, binaries: general

1. Introduction

The superluminous star η Carinae has been observed by nearly every X-ray satellite flown. *EINSTEIN* observations (Seward et al. 1979; Seward and Chlebowski 1982; Chlebowski et al. 1984) first resolved the star's X-ray emission from the rest of the Carina Nebula and mapped out point-like emission centered on the star and an elliptical X-ray ring around the star extending out to $\sim 15''$. *GINGA* (Koyama et al. 1990) and *BBXRT* provided the first clear measures of the strong Fe K line indicative of thermal emission probably produced by shocked gas. *ROSAT* discovered the variable nature of the hard source (Corcoran et al. 1995), while *ASCA* discovered $\geq 50\times$ solar abundance of nitrogen (Tsuboi et al. 1997) in the outer homunculus and fluorescent Fe K emission (Corcoran et al. 1998) unresolved from the strong thermal line. A hard X-ray tail extending to ~ 50 keV was observed with the *BeppoSAX* Phoswich Detector System (Viotti et al. 2001). A 2-10 keV X-ray lightcurve obtained by *RXTE* (consisting typically of 1 observation per week since 1996) revealed small amplitude periodic flares with $P = 85$ days (Corcoran et al. 1997) and confirmed that the variability seen in 1992 by *ROSAT* recurred (Ishibashi et al. 1999; Corcoran et al. 2001) on the same 5.5 year period which fits the He I 10830Å line variability reported by Damineli (1996). These recent X-ray measurements along with variations in the radio (Duncan et al. 1995) and near-IR (Damineli et al. 2000) all suggest that η Carinae may be the Galaxy's most massive binary system (Damineli, Conti and Lopes 1997; Corcoran et al. 2001) in which the hard X-ray emission is produced by shocked gas in the region where the wind from η Carinae collides with the wind from the companion star. An early observation of η Carinae by the Advanced CCD Imaging Spectrometer (ACIS) on *CHANDRA* in September 1999 (Seward et al. 2001) provided the first image of the X-ray regions at a resolution of $\approx 1''$, though, due to degradation produced by charged particle damage of the CCDs, this observation could not be precisely calibrated spectrally.

Here we report the first calibrated observation of η Carinae with the High Energy Transmission Grating Spectrometer (HETGS, Canizares et al. 2001, in preparation) on the *CHANDRA* X-ray observatory (Weisskopf, O'Dell, & van Speybroeck 1996) using the ACIS linear array (ACIS-S) to read out the dispersed spectrum. The *CHANDRA* HETGS is well suited for observing the point-like hard emission from η Carinae for two reasons: 1) the spectral energy distribution of the emission fits nicely in the HETGS bandpass and 2) this emission is thought to be dominated by thermal processes which should produce strong line emission in the dispersed spectrum. Our deep (24.9 hour) observation of η Carinae with the HETGS provides the first spectrally-resolved measure of the X-ray spectrum, allowing for the first time a detailed definition of the temperature distribution,

density, and chemical abundance of the hot, unresolved emission from the star. In this first report we discuss the overall spectral morphology of the unresolved X-ray emission, examine the emission line temperature and density diagnostics, and provide an uninterrupted lightcurve of the unresolved X-ray source over the length of the observation.

2. The Observation

The *CHANDRA* HETGS+ACIS-S observation of η Carinae was performed on 19 November 2000 – 20 November 2000. The total exposure time of the observation was 89,546 seconds. The spacecraft roll was chosen so as to avoid contamination of the dispersed spectra by other bright X-ray sources in the field. The data were cleaned and processed using the standard pipeline processing available at the *CHANDRA* X-ray Center. Images and spectra were extracted from the level 1.5 events using the Chandra Interactive Analysis of Observations (CIAO) analysis package.

The zeroth-order image, color-coded by X-ray energy is shown in figure 1. This image is similar to that previously published (Seward et al. 2001) though the energy calibration is better in the new image. In particular, the ACIS-S zeroth-order image shows the soft elliptical "shell" of emission surrounding the hard X-ray core, which is unresolved to ACIS at scales of $\sim 0.5'' \approx 10^{16}$cm ≈ 1000 AU. The X-ray flux in the elliptical "shell" is very non-uniform, bright in the south and west (near the "S-ridge" and the "W-condensations" in the outer debris field, Walborn, Blanco & Thackary 1978) and faint in the north and east. The hard, unresolved "core" appears to be surrounded by a halo of X-ray emission at moderate X-ray energies (though the apparent emission at distances between $2.5''$ and $5''$ is probably consistent with the point-spread of the mirror+detector, Seward et al. 2001).

3. The X-ray Grating Spectrum of η Carinae

The ACIS-S image of the dispersed spectrum shows that the hard source is unresolved to *CHANDRA*; in particular, there is no observed dispersed spectrum from any other source of emission in the ACIS-S field aside from the unresolved, hard core source associated with η Carinae. We extracted the dispersed medium energy grating (MEG) and high energy grating (HEG) spectra from the X-ray event file using CIAO. Both plus and minus orders for the first, second and third order MEG and HEG source spectra were extracted, along with appropriate background spectra. Figure 2 shows the MEG +1 order spectrum, while figure 3 shows the HEG +1 order in the vicinity of the Fe K line. The MEG and HEG spectra of η Carinae represent the first calibrated high resolution X-ray spectra of this star uncontaminated by extended soft emission. The MEG spectrum shows very little emission from the unresolved source at energies less than 1.5 keV ($\lambda > 8.5$ Å) due to strong absorption, and reveals a significant X-ray continuum in the $1 - 8$Å range and the presence of strong line emission from lines of S XV-XVI, Si XIII-XIV, Mg XII, Ca XIX, and Fe

K. Strong forbidden lines of S XV, Si XIII and Mg XII were detected. In the HEG spectrum, the Fe line region shows a thermal emission line produced by Fe XXV and a blend of fluorescent Fe I Kα_1+Kα_2 lines centered at 1.94Å.

3.1. Modelling the Spectrum

We attempted to fit the MEG spectrum with a combination of optically-thin thermal emission models using the XSPEC analysis package (Arnaud 1996). Because the dispersed spectrum has many bins with few counts and because background does not contribute significantly in the energy range of interest ($E > 1.5$ keV or $\lambda < 8$ Å), we used a modified version of the "C-statistic" (Cash 1979) on the total (non-background-subtracted) spectrum instead of the χ^2 statistic. Previous analyses indicated that the emission at energies above 1.5 keV could be fit by emission at a single temperature (for eg., Corcoran et al. 2000). As shown in Figures 4 and 5, a variable abundance single temperature thermal model (VMEKAL-XSPEC, Mewe, Kaastra & Liedahl 1995) provided a good fit to the continuum emission and most of the resolved emission lines. The parameters of the best fit single component model are given in Table 1. The single component temperature is $kT = 4.4$ keV with a column density of $N_H = 4.9 \times 10^{22}$ cm^{-2}, in reasonable agreement with earlier results. However, we found that no isothermal model could simultaneously match the strengths of the H-like and He-like lines of Si in the 4.5Å $< \lambda <$ 6Å range. Fitting both the He-like and H-like ions required the addition of at least one additional thermal component. Our best fit 2-temperature model is given in table 2 and shown in figures 4 and 5. This 2-temperature model adequately matches the strength of both the He-like and H-like lines. This is the first time that the unresolved X-ray emission from η Carinae has been shown to require a non-isothermal temperature distribution. The maximum temperature we derive, $kT \approx 8.7$ keV, is nearly a factor of 2 larger than most other published temperatures for η Carinae, and to our knowledge represents the highest temperature ever associated with an early-type star.

In our modelling of the X-ray spectrum we held most elemental abundances at their solar values (Anders & Grevesse 1989), but allowed the abundances of Si, S and Fe (all of which have strong lines in the X-ray spectrum) to vary. The derived abundances for the 1 and 2 temperature models for these 3 elements are given in table 1. In each case the abundances of the Si, S, and Fe were slightly non-solar: Si was found to be slightly overabundant, S significantly overabundant (by about 70%), while Fe was slightly underabundant.

3.2. The He-like Lines and the f/i Ratio

The ratio of the intensity of the forbidden component to the intercombination component of the He-like lines (the f/i ratio) is a density diagnostic (Gabriel & Jordan 1969), though the ratio may be also increased by UV photoexcitation (Kahn et al. 2001) which can suppress the forbidden

line and enhance the intercombination line. We fit the Si XIII, S XV and Fe XXV lines in XSPEC by first isolating the wavelength region around the line complex of interest and using gaussians to model the lines with inclusion of a power law component to describe the background. The fits are shown in figures 6–8 and the fit parameters are given in Table 2. The intercombination lines for all three ions are weak and our analysis only yields upper limits for the intensities of these lines. We measure f/i values of > 1.0 for Si XIII, > 2.0 for S XV and > 2.1 for Fe XXV. These values correspond to electron densities of $< 10^{14}$ cm^{-3} for Si XIII and $< 10^{15}$ cm^{-3} for S XV and Fe XXV.

3.3. The Fe Fluorescent Line

We fit the Fe I fluorescent line from the HEG spectrum in XSPEC by isolating the Fe K region and using a single gaussian line plus power-law background component. The line parameters are given in Table 2. The measured equivalent width of the line is only 39 eV, which is about half the value of the smallest equivalent width seen by *ASCA* (Corcoran et al. 2000).

4. The X-ray Lightcurve

Though η Carinae is known to undergo significant increases (or "flares") in its 2-10 keV X-ray flux, sometimes increasing in flux by $20 - 50\%$ on a timescale of many days (Corcoran et al. 1997; Ishibashi et al. 1999), no short-term variability on timescales less than a day has ever been detected. The best previous measure of the X-ray lightcurve from η Carinae was a long (~ 100 ksec) *ASCA* observation spanning some 2.5 days which did not find any significant variability in the 2-10 keV X-ray emission (Corcoran et al. 1998). We can re-examine the issue of η Carinae's short-term X-ray variability using our *CHANDRA* data, since this observation provides a unique uninterrupted view of the source for a period of about a day. We first extracted a lightcurve from the zeroth-order image on the S3 chip using a circular $5''$ diameter region centered on the unresolved source. We also extracted a background lightcurve from a source free circular region of diameter $17''$ centered just beyond the outer elliptical emission region surrounding the hard unresolved source. The net (background-subtracted) X-ray lightcurve of the unresolved source in the zeroth order data is shown in figure 9a. While there is little evidence for variability in this zeroth order lightcurve, the counting rate for the central source in zeroth-order is large enough (~ 0.2 counts s^{-1}) that event pileup is a problem. From the continuous clocking data published by Seward et al. (2001) the unpiled rate of the central source is 1.6 ACIS-I counts s^{-1}, which implies that the unpiled rate in the ACIS-S zeroth order image is ~ 0.8 counts s^{-1}, suggesting a pileup fraction of $\sim 75\%$. In addition to reducing the observed count rate, this degree of pileup will severely dampen any real source variability in the zeroth-order data. We used the count rate/pileup estimator tool provided by the *CHANDRA* X-ray center to estimate the sensitivity to source variability in the zeroth-order data and found that, for a source spectrum described by the fit to the dispersed spectrum of the central source, variations of the central source flux by about a factor of 3 imply a change in observed (piled-up) count rate

of only 30%. Thus, slight variations in the observed ACIS-S+HETG zeroth order lightcurve might imply much larger flux variations in the source, if this analysis is reliable.

To further investigate any possible variations in the hard X-ray emission from η Carinae for the duration of the *CHANDRA* observation, we extracted a lightcurve from the dispersed spectrum of the central source. Since the dispersed spectrum is spread over a large number of detector pixels, event pileup is not significant. To avoid problems caused by differing chip sensitivities and backgrounds, we considered only the MEG minus-order data from the ACIS-S2 chip. We extracted all dispersed counts in the MEG-minus order from a narrow rectangular region centered on the dispersed spectrum, and extracted background in a similar region offset from the dispersed spectrum. In the region used for source extraction the maximum number of counts per unbinned ACIS-S2 pixel was 19 counts, which corresponds to an observed count rate of 2×10^{-4} counts s^{-1}, or 6×10^{-4} counts per readout frame. Figure 9b shows the net lightcurve of the dispersed MEG minus-order spectrum from chip S2. This lightcurve shows little evidence of variability, suggesting that η Carinae did not undergo any real coherent variations during the *CHANDRA* observation.

5. Discussion

Recent evidence suggests that η Carinae may be a massive binary star, in which variable X-ray emission is produced by shocked gas at the interface where the wind from η Carinae collides with the wind of its companion (presumably some less massive early-type star). The line complexes resolved in the HETGS spectra provide unique information about the physical condition of the X-ray emitting region and thus on the single or binary nature of η Carinae. In the colliding wind model the wind from η Carinae forms a bow shock around the companion, since the companion's wind is probably weaker than η Carinae's wind, i.e. $\eta \equiv (\dot{M}V_\infty)_c/(\dot{M}V_\infty)_\eta < 1$; here $\dot{M}$ represents the wind mass loss rate and V_∞ the wind terminal velocity, and the subscripts η and c refer to η Carinae and the companion, respectively. In published models (Damineli et al. 2000; Corcoran et al. 2001) the mass loss rate from η Carinae is thought to be at least a factor of 10 larger than that of the companion, while the terminal velocities are probably within a factor of 3 (see below), so that $\eta < 0.3$.

The mere presence of numerous strong emission lines confirms that the X-ray emission is dominated by thermal processes from shocked gas. The dominance of thermal processes in the *CHANDRA* energy range suggests that there is little or no contribution from non-thermal processes (which could be produced via inverse compton scattering of photospheric UV photons if Fermi acceleration of the electron population in the shock is important). The temperature distribution of the X-ray emission as measured by *CHANDRA* provides a measure of the pre-shock wind velocities for both stars. In a colliding wind binary, the temperature of the shocked gas facing either star is kT (keV) $\approx 2.59\mu V^2$ (see the eq. 51 in Usov (1992)) where μ is the mean mass per particle and V is the stellar wind speed in 1000 km s^{-1}. For simplicity we assume $\mu \approx 1$, though this value may not be truly representative of the chemical composition of the wind of either η Carinae or its

companion. We neglect the motion of the shock stagnation point due to the orbital motion of the stars, since orbital motion has a significant influence on the derived temperatures only when the stars are near periastron (and the stellar velocities are greatest), while the HETGS observation was obtained near apastron according to the ephemeris of Corcoran et al. (2001). The temperatures we derived, $kT \approx 1.1$ and ≈ 8.7 keV, suggest velocities of ~ 700 km s^{-1} and ~ 1800 km s^{-1}. The speed of the wind from η Carinae is thought to be ~ 500 km s^{-1} (Hillier et al. 2001), fairly consistent with the lower velocity we derive from our X-ray analysis. A velocity of ~ 500 km s^{-1} is sufficient to produce the $kT \sim 1$ keV emission, but cannot produce the hotter emission revealed in the MEG spectrum. Naively, we interpret the low-temperature component as shocked emission from the relatively slow wind of η Carinae, and the high-temperature component as shocked emission by the faster wind from the companion star, so that $V_{\infty,\eta} \approx 700$ km s^{-1} and $V_{\infty,c} \approx 1800$ km s^{-1}.

The f/i ratios derived from our analysis of the He-like ions are large, and show that the line forming region has a density $n_e < 10^{14}$ cm^{-3} and that enhancement of the intercombination component by UV photoexcitation is unimportant. This suggests that the line forming region is located far from the stellar photosphere, where wind densities and UV fluxes are low. This is broadly consistent with published descriptions of the orbit (Damineli et al. 2000; Corcoran et al. 2001) in which the shocked emission forms far from either star (though closer to the companion than to η Carinae) in a region of low particle and UV photon density. In the colliding wind model, the apex of the bow shock is located at a distance of $d/(1+\sqrt{\eta})$ from η Carinae, where d is the separation of the two stars. At the phase of the *CHANDRA* observation, $\phi = 0.60$, the two stars are separated by about 4×10^{14} cm, using the orbital elements of Corcoran et al. (2001). At this time the bow shock is about 2.5×10^{14} cm from η Carinae, and about 1.5×10^{14} cm from the companion. The density of the wind at a distance r from the photosphere is $n = \dot{M}/(4\pi r^2 V \mu m_H)$, where $\dot{M}$ is the mass loss rate and V the wind velocity. Using $\dot{M}_\eta = 10^{-4} M_\odot$ yr^{-1} and $V_{\infty,\eta} \approx 500$ km s^{-1} (Hillier et al. 2001), then the density of the wind from η Carinae at a distance of 2.5×10^{14} cm is only $n \approx 8 \times 10^8$ cm^{-3}. Using $\dot{M}_c = 10^{-5} M_\odot$ yr^{-1} (Corcoran et al. 2001) and $V_{\infty,c} = 1800$ km s^{-1} as appropriate values for the companion's wind, the density of the companion's wind at a distance $r = 1.5 \times 10^{14}$ cm is also only about 10^8 cm^{-3}. The predicted densities are consistent with the upper limits derived from our analysis of the f/i line intensity ratios. However, if the actual density of the emission region is near the limit implied by the f/i ratios, this might indicate that the assumed wind momentum balance is not quite right.

In contrast, newly published X-ray grating spectra of θ^1 Ori C (Schulz et al. 2000), ζ Ori (Waldron & Cassinelli 2001) and ζ Pup (Kahn et al. 2001) all have f/i ratios which are lower than the values we derive from the η Carinae X-ray line spectrum. None of these stars are known to show any colliding wind effects, and apparently, in these massive stars, the X-ray lines form relatively near the stellar photosphere, probably within a few stellar radii. This is not the case for η Carinae.

The strength of the Fe fluorescent line is related to the column density of scattering material by $EW \approx 2.3 N_{24}$ keV, where EW is the equivalent width of the line in keV and N_{24} the total column density of cold material in units of 10^{24} cm^{-2} (Kallman 1995). The *ASCA* spectra suggest

that $EW \approx 4-7N_{24}$ for η Carinae outside of eclipse (Corcoran et al. 2000). Thus at the time of the HETGS observation the equivalent width of the Fe fluorescent line implies $N_{24} \approx 0.01 - 0.03$, i.e. that the column density of cold material is $N_H \approx 1-3 \times 10^{22}$ cm^{-2}. This value is in fair agreement with the value of $N_H = 5 \times 10^{22}$ derived from fitting the X-ray continuum in the MEG spectrum, suggesting that some of the same material which produces the X-ray absorption also is responsible for producing the Fe fluorescent emission. The equivalent width of the line which we derive here is much smaller than any values given in either Corcoran et al. (2000) or Corcoran et al. (1998). This may be the result of the difficulty in determining the actual width of the fluorescent line in the *ASCA* spectra since the line is not resolved from the thermal component. However, if this variation is real, it may represent a real decrease in the scattering optical depth. Such a decrease is not unexpected in the binary model since at the time of the HETGS observation, the companion is nearly in front. Since the companion's wind is less dense this could produce a decrease in the scattering optical depth at the time of the HETGS observation.

6. Conclusions

We have presented here the first high-energy X-ray grating spectrum of the supermassive star η Carinae. This grating spectrum shows strong line emission from H-like and He-like ions of S, Si, Mg, Ca, and Fe, and confirms the presence of the Fe fluorescent line discovered by *ASCA*. The forbidden lines of the He-like ions are strong and the intercombination lines weak, indicating that the line forming region is far from the stellar photosphere. These results are all consistent with the current picture of η Carinae as a colliding wind binary. We expect that interesting variations in the X-ray spectrum will occur as the two stars approach periastron (which should next occur on June 20, 2003). In particular, we expect that the strength of the forbidden lines will weaken near periastron, as the density in the X-ray region increases and as the UV photospheric flux in the line region intensifies. Additional HETGS observations as the stars approach periastron, especially in conjunction with UV spectroscopy, will provide unique and significant constraints on the orbital geometry, the strengths of the winds from both stars, and the evolutionary stages of the stellar components.

We would like to thank Fred Seward for important contributions to this paper, in particular in emphasizing the importance of pileup in measuring the variation of the central source. We also gratefully acknowledge the *CHANDRA* staff at the SAO/CfA and the HETGS team at MIT for their help in scheduling the observation and in analyzing the data. We made use of the FTOOLS suite of software supported by the HEASARC. This research has made use of NASA's Astrophysics Data System Abstract Service.

REFERENCES

Anders, E. & Grevesse, N., 1989, Geochimica et Cosmchimica Acta, 53, 197

Arnaud, K. A., 1996, in Astronomical Data Analysis Software and Systems V, eds. Jacoby G. and Barnes J., p17, ASP Conf. Series volume 101.

Chlebowski, T., et al., 1984, ApJ, 281, 665

Cash, W. 1979, ApJ, 228, 939

Corcoran, M. F., et al., 1995, ApJ, 445, L121

Corcoran, M. F., et al., 1997, Nature, 390, 587

Corcoran, M. F., et al., 1998, ApJ, 494, 381

Corcoran, M. F., et al., 2000, ApJ, 545, 420

Corcoran, M. F., Ishibashi, K., Swank, J. H., and Petre, R., 2001, ApJ, 547, 1034

Damineli, A., 1996, ApJ, 460, L49

Damineli, A., Conti, P. S., Lopes, D. F., 1997, New Astronomy, 2, 107

Damineli, A., Lopes, D. F., and Conti, P. S., 1999, in ASP. Conf. Ser. 179, η Carinae at the Millennium,, ed. J. A. Morse, R. M. Humphreys, and A. Damineli (San Francisco: ASP), 288

Damineli, A., Kaufer, A., Wolf, B., Stahl, O., Lopes, D. F., Araújo, F. X., 2000, ApJ, 528, L101

Duncan,R.A., et al., 1995, ApJ, 441, L73

Gabriel, A. H., and Jordan, C., 1969, Nature, 221, 947

Hillier, D. J., Davidson, K., Ishibashi, K., and Gull, T., 2001, ApJ, submitted

Ishibashi, K., et al., 1999, ApJ, 524, 983

Kahn, S. M., Leutenegger, M. A., Cottam, J., Rauw, G., Vreux, J. -., den Boggende, A. J. F., Mewe, R., & Güdel, M. 2001, A&A, 365, L312

Kallman, T., 1995, ApJ, 455, 603

Koyama,K., et al., 1990, ApJ, 362, 215

Mewe, R., Kaastra, J. S., & Liedahl, D. A. 1995, Legacy, 6, 16

Pittard, J. M., Stevens, I. R., Corcoran, M. F., and Ishibashi, K., 1998, MNRAS, 299, L5

Schulz,N.S., Canizares,C.R., Huenemoerder,D., Lee,J.C., 2000, ApJ, 545, L135

Seward, F. D., Seward,F.D., Forman,W.R., Giacconi,R., Griffiths,R.E., Harnden,F.R.,Jr., Jones,C., and Pye,J.P, 1978, ApJ, 234, L55

Seward, F. D., and Chlebowski, T. 1982, ApJ, 256, 530

Seward, F. D., Butt, Y. M., Karovska, M., Prestwich, A., Schlegel, E. M., and Corcoran, M., 2001, ApJ, 553, 832

Tanaka, Y., Inoue, H., Holt, S. S., 1994, PASJ, 46, L37

Tsuboi, Y., et al., 1997, PASJ, 49, 85

Usov, V. V., 1992, ApJ, 389, 635

Viotti, R. F., Antonelli, L. A., Corcoran, M. F., Damineli, A., Grandi, P., Muller, J. M., Rebecchi, S., Rossi, C. and Villada, M., 2001, A&A, submitted

Walborn, N. R., Blanco, B. M., & Thackeray, A. D. 1978, ApJ, 219, 498

Waldron, W. L. & Cassinelli, J. P. 2001, ApJ, 548, L45

Weisskopf, M. C., O'Dell, S. L., & van Speybroeck, L. P. 1996, in Proc. SPIE, 2805, 2

Figure 1. Zeroth order image, color coded for X-ray energy (red - low energy; green - moderate energy; blue - high energy). The diagonal band at the top of the image is the dispersed medium energy grating (MEG) spectrum.

Figure 2. +1 order Medium Energy Grating (MEG) spectrum of η Carinae. Strong lines from H- and He-like ions of Mg, Si, S, Ca and Fe are indicated. For comparison the spectrum of the background is also shown; background only contributes about 1 count in each spectral bin.

Figure 3. Iron K line region from the +1 order High Energy Grating (HEG) spectrum of η Carinae. Emission is seen from He-like iron originating in gas at a temperature of $\sim$ 8 keV. In addition fluorescent line emission from cool iron is also clearly detected. The spectrum at the bottom is the X-ray background spectrum.

Figure 4. Fits to the MEG +1 order spectrum. A two-temperature fit using a variable abundance collisionally ionized plasma model (VMEKAL-XSPEC, Mewe, Kaastra & Liedahl 1995) is shown in blue, and a single-temperature fit with the same emission model is in red. The single temperature model cannot reproduce simultaneously the strength of the S XV, Si XIII and Si XIV lines in the range 4.5–7.0Å.

Figure 5. Same as in Figure 4, but emphasizing the S & Si line region.

Figure 6. Fit to the f, i, r lines of Si XIII.

Figure 7. Fit to the f, i, r lines of S XV.

Figure 8. Fit to the f, i, r lines of Fe XXV (near 1.85Å) and the Fe I fluorescent line (at 1.93Å).

Figure 9a. The background-corrected lightcurve of the unresolved hard source derived from the zeroth-order data. Event pileup is severe (the pileup fraction is about 75%), which will severely reduce the observed amplitude of any real source variability.

Figure 9b. The background-corrected lightcurve of the unresolved hard source derived from the dispersed MEG minus order for events falling on the S2 chip. Event pileup is not significant in the dispersed data.

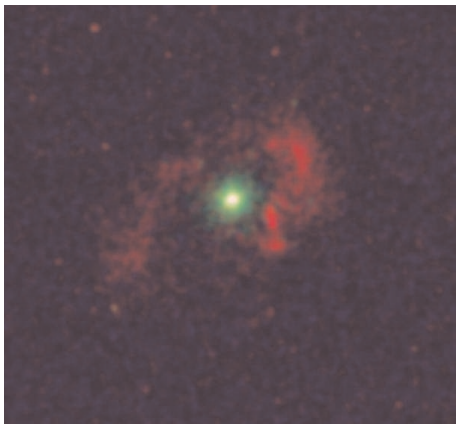

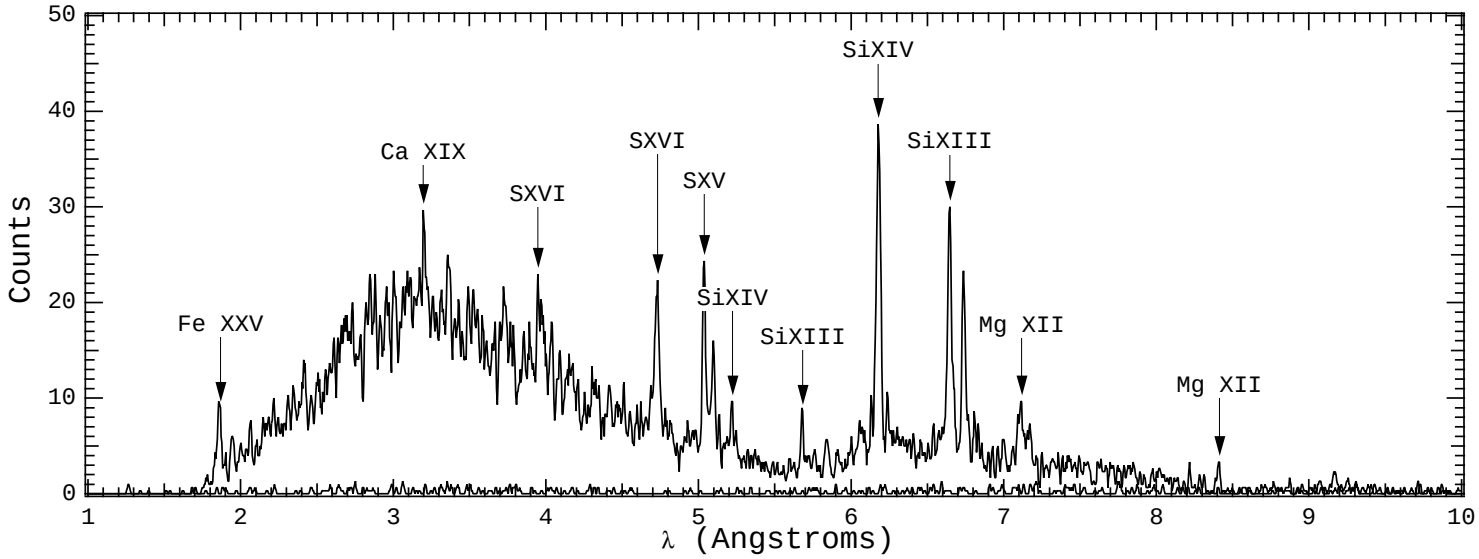
Counts
λ (Angstroms)
Fe XXV
Ca XIX
SXVI
SXVI
SXV
SiXIV
SiXIV
SiXIII
SiXIII
Mg XII
Mg XII

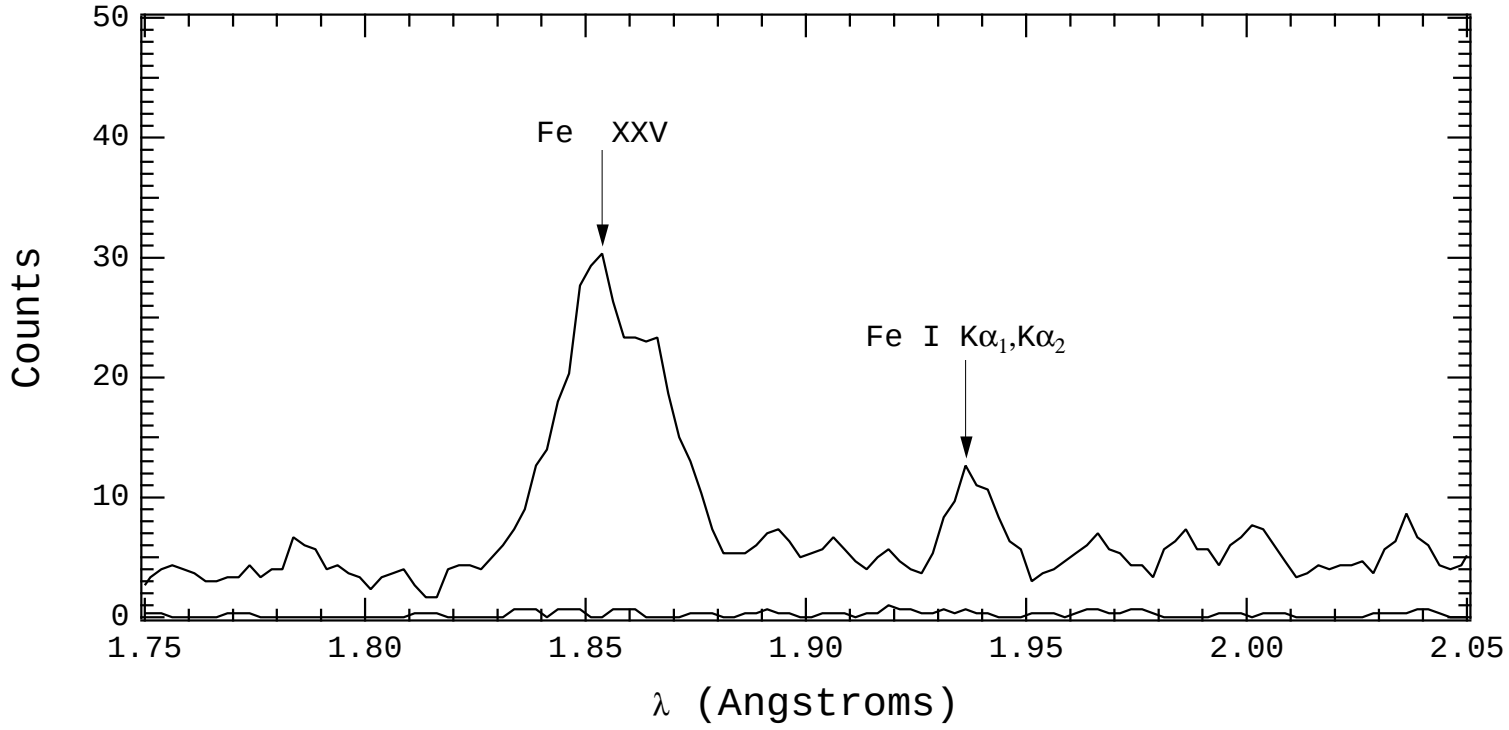
Counts
50
40
30
20
10
0
Fe XXV
Fe I Kα1,Kα2
1.75
1.80
1.85
1.90
1.95
2.00
2.05
λ (Angstroms)

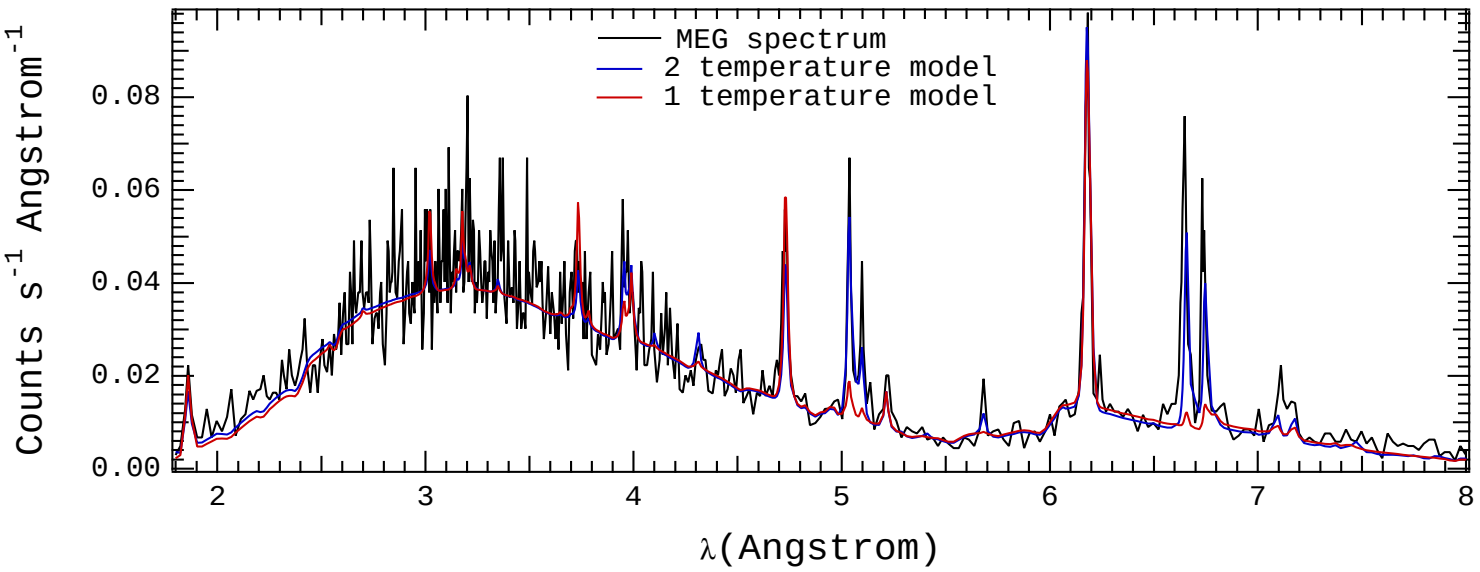
MEG spectrum
2 temperature model
1 temperature model
Counts s^{-1} Angstrom^{-1}
0.00
0.02
0.04
0.06
0.08
2
3
4
5
6
7
8
λ(Angstrom)

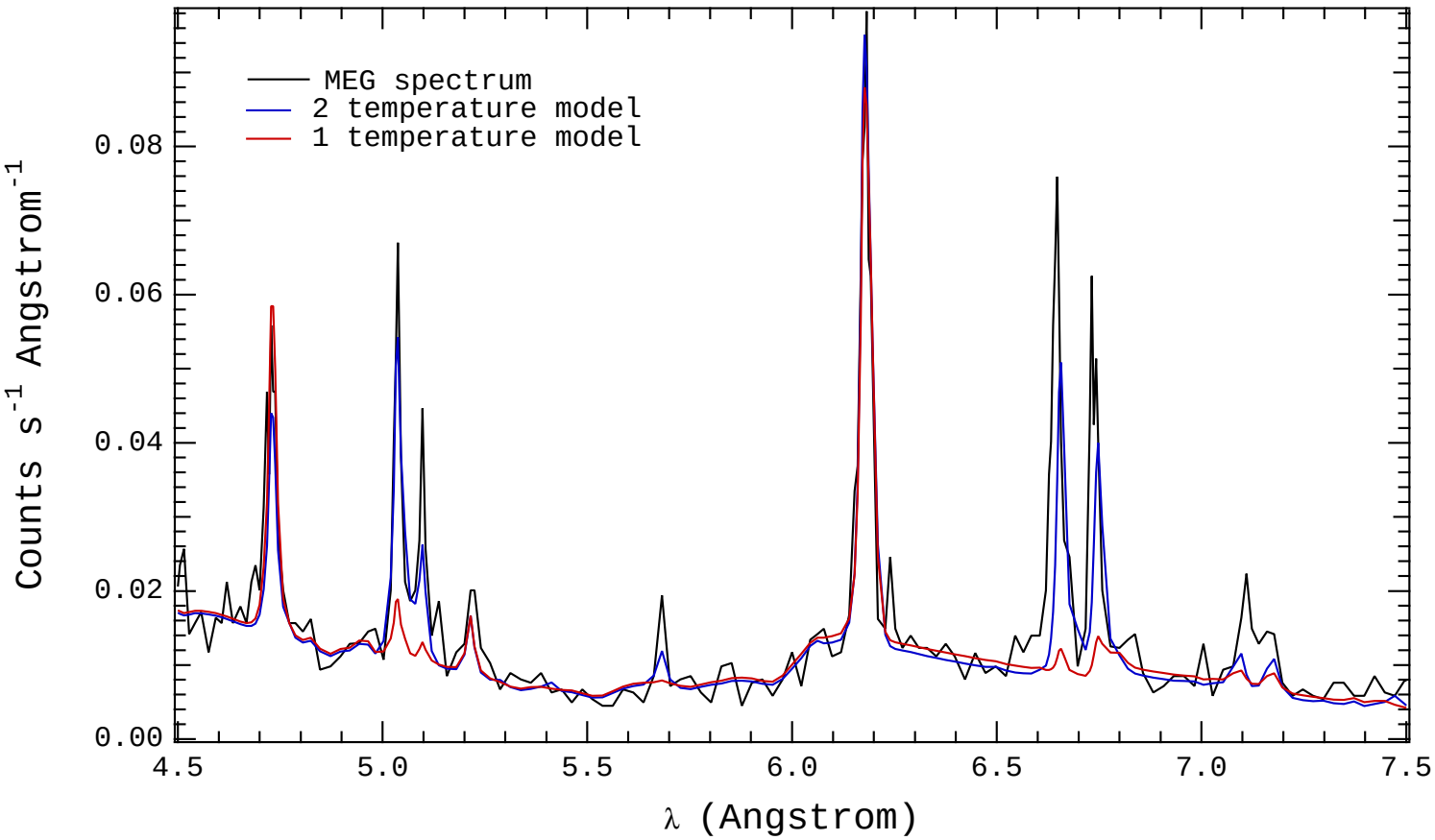
MEG spectrum
2 temperature model
1 temperature model
Counts s-1 Angstrom-1
0.00
0.02
0.04
0.06
0.08
4.5
5.0
5.5
6.0
6.5
7.0
7.5
λ (Angstrom)

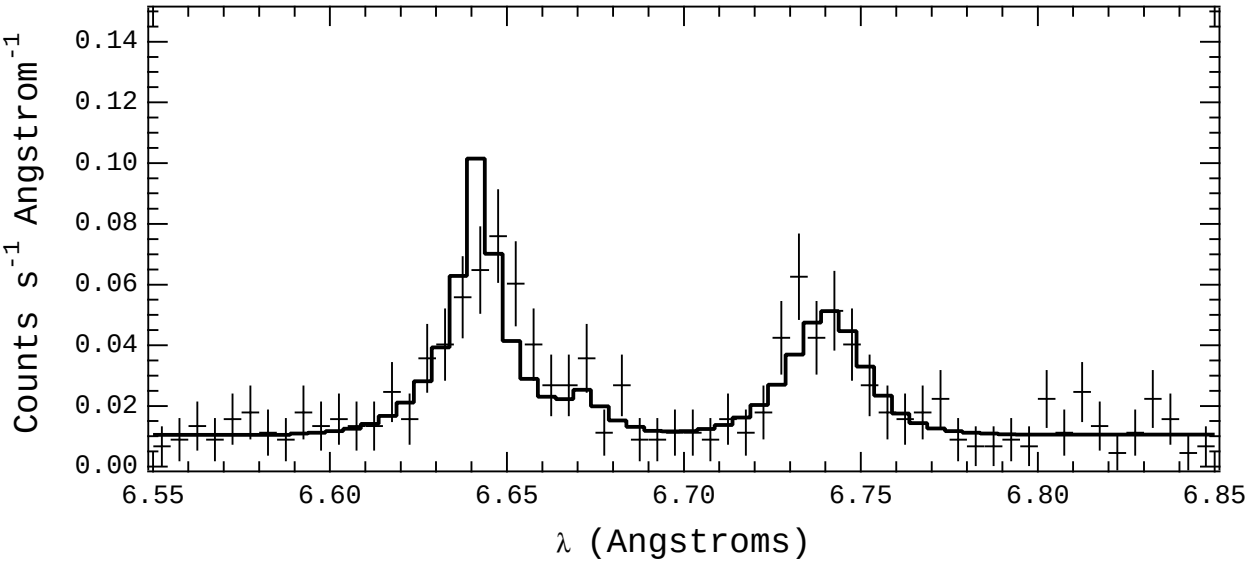
Counts s^{-1} Angstrom^{-1}
0.14
0.12
0.10
0.08
0.06
0.04
0.02
0.00
6.55
6.60
6.65
6.70
6.75
6.80
6.85
λ (Angstroms)

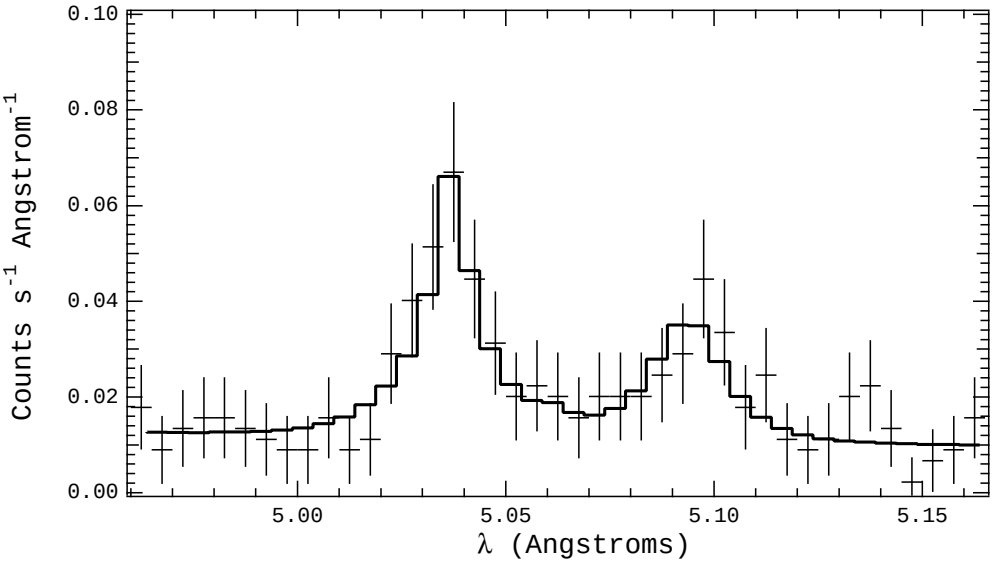
0.10
0.08
0.06
0.04
0.02
0.00
Counts s^{-1} Angstrom^{-1}
5.00
5.05
5.10
5.15
λ (Angstroms)

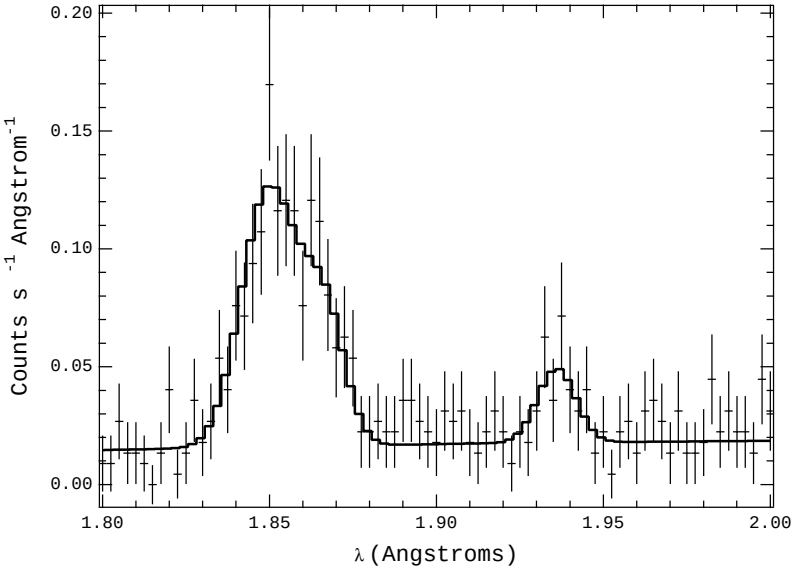
0.20
0.15
0.10
0.05
0.00
Counts s -1 Angstrom-1
1.80
1.85
1.90
1.95
2.00
λ(Angstroms)

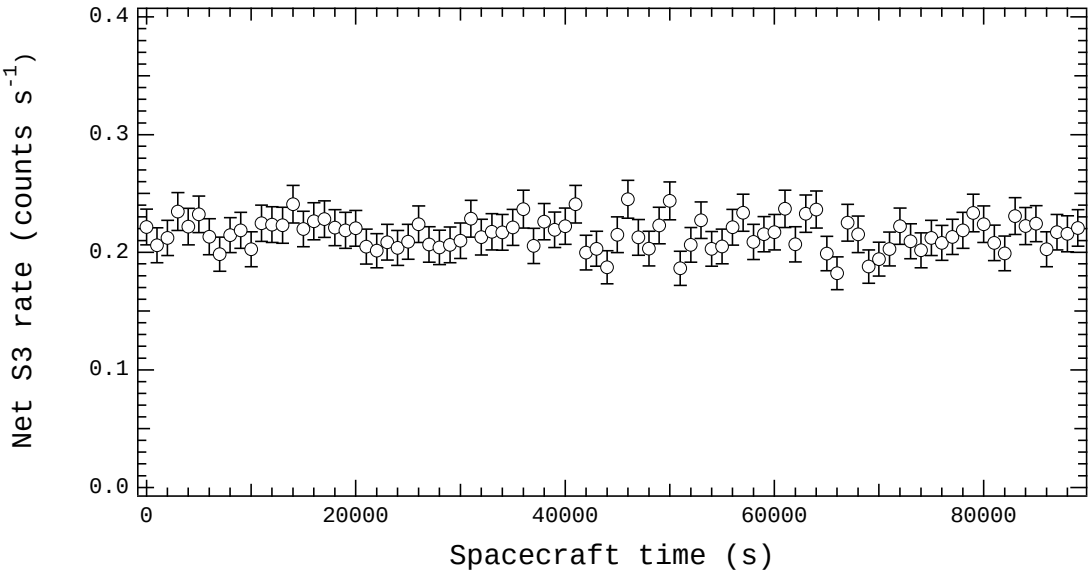
Net S3 rate (counts s^{-1})
0.0
0.1
0.2
0.3
0.4
0
20000
40000
60000
80000
Spacecraft time (s)

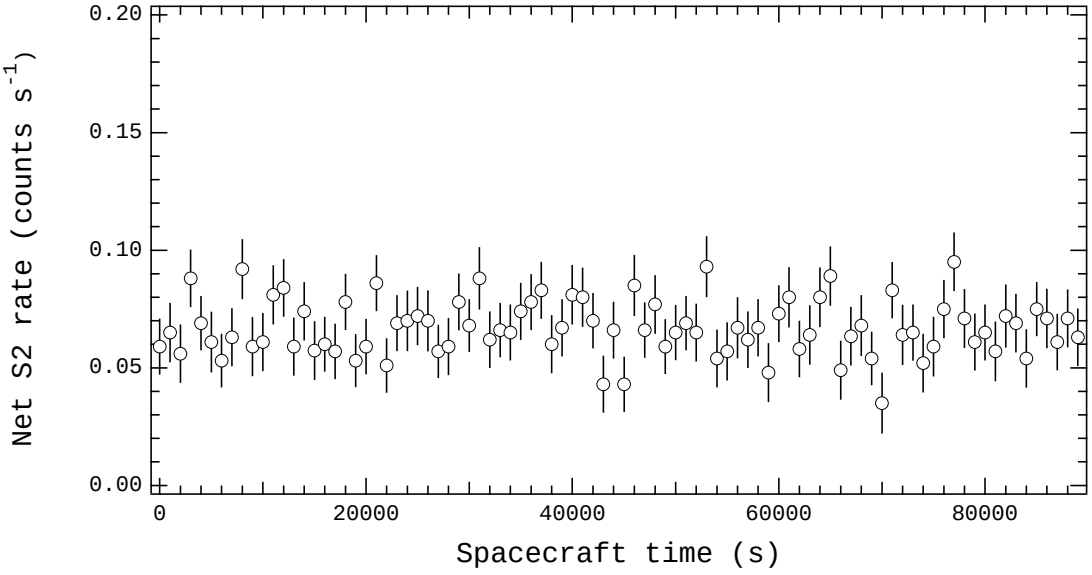
0.20
0.15
0.10
0.05
0.00
Net S2 rate (counts s-1)
0
20000
40000
60000
80000
Spacecraft time (s)

Table 1.

Parameter	Units	1 Component Fit	2 Component Fit
N_H	10^{22}cm^{-2}	4.9	5.1($\pm$0.4)
kT	keV	4.4	1.1($\pm$0.1)
Emission Measure[1]	10^{57}cm^{-3}	4.0	1.8($\pm$0.1)
Lx (2-10, absorbed)[1]	ergs s^{-1}	2.6	3.0
Lx (2-10, unabsorbed)[1]	10^{34}ergs s^{-1}	3.9	4.5
Si/Si$_\odot$		1.5	1.1($\pm$0.2)
S/S$_\odot$		1.4	1.7($\pm$0.4)
Fe/Fe$_\odot$		0.6	0.9($\pm$0.2)
kT_2	keV		8.7($\pm$1.7)
Emission Measure[1] $_2$	10^{57}cm^{-3}		2.9($\pm$0.3)
$C-$statistic		2035	1619

[1] calculated assuming a distance of 2100 pc (Corcoran et al. 2001)

Table 2.

Line	E (keV)	Measured E (keV)	Eq. Width (eV)	Intensity (photons s^{-1} cm^{-2})
SiXIII (r)	1.864	1.866	38	0.009
SiXIII (i)	1.853	1.859	< 4.3	< 0.002
SiXIII (f)	1.839	1.839	21.4	0.002
SXV (r)	2.460	2.460	33.1	0.009
SXV (i)	2.450	2.450	< 6.0	< 0.001
SXV (f)	2.431	2.434	25.6	0.002
FeXXV (r)	6.700	6.700	261	0.034
FeXXV (i)	6.682	6.680	< 42	< 0.007
FeXXV (f)	6.636	6.640	42	0.015
FeI	6.424	6.407	39.4	0.009